UDC 621.351/.355 doi: 10.15407/Surface.2023.15.185

HIGH-PERFORMANCE $LiMn_2O_4$/GRAPHENE COMPOSITE FOR LITHIUM-ION BATTERIES

Yu.V. Shmatok, N.I. Globa, V.A. Sirosh, S.A. Kirillov

Joint Department of Electrochemical Energy Systems of the NAS of Ukraine, 38A Vernadsky Ave., 03680, Kyiv, Ukraine, e-mail: yu.shmatok@gmail.com

The improvement of the electrochemical characteristics of lithium-manganese spinel $LiMn_2O_4$ is one of the most important tasks for researchers in the field of lithium-ion batteries. Graphene materials can have a positive effect on the functional characteristics of $LiMn_2O_4$-based composite electrodes due to their unique properties. Therefore, the composite electrodes based on spinel $LiMn_2O_4$ with commercial samples of graphene nanoplatelets were investigated. Structural, morphological and surface characteristics of $LiMn_2O_4$ and graphene samples studied using X-ray diffraction, scanning electron microscopy and nitrogen adsorption–desorption methods. Electrochemical test of the composite electrodes was performed in CR2016 coin cells with lithium metal anode. It is shown that the nature of $LiMn_2O_4$ is the main factor that determines electrochemical behavior of composite electrodes in terms of their cycling stability and rate capability. At the same time, the influence of graphene type within one spinel is relatively small, but the presence of graphene is important to ensure the required level of conductivity of the electrode structure. Despite the lower initial specific capacity, the composites with $LiMn_2O_4$ sample synthesized by a citric acid-aided route demonstrate better cycling stability and higher maximum discharge currents up to 40 C compared to composites based on $LiMn_2O_4$ synthesized by a solid-state method. The electrochemical characteristics obtained are in good agreement with the results of electrochemical impedance spectroscopy.

Keywords: *lithium-manganese spinel, graphene nanoplatelets, composite electrode, charge transfer, cyclability, rate capability, exchange current.*

Introduction

Optimizing the electrode-electrolyte structure is one of the ways to increase the specific characteristics of lithium-ion batteries (LiBs). This can be achieved both due to the improvement of the electrode manufacturing technology and by changing the components that make up the electrodes. In view of this, among many carbon materials, graphenes are considered as the promising components of the electrode of LiBs [1-3]. The attractiveness of graphene is due to their physical and chemical properties, such as: a significant specific surface area (up to 2630 m^2/g), high intrinsic charge carrier mobility (350 000 $cm^2/V \cdot s$) and high thermal conductivity (~3000 W/m·K) [4]. The ability of graphene to form 3D structures allows reducing the charge transfer resistance in the porous structure of the electrodes and contributes to increasing their mechanical stability [5]. This is important in view of the volumetric changes characteristic of most electrodes during lithium intercalation/deintercalation.

Modern methods of graphene synthesis and modification make it possible to create composite electrodes with high electronic conductivity and accelerated lithium cation diffusion [6]. In addition, the positive effect of using graphene as part of the electrode also consists in the formation of a more effective solid electrolyte interface at the boundary of the electrode/electrolyte phase distribution [7]. As a result, the specific capacity of composite electrodes preserves even at a significant discharge rates and low operating temperatures. Graphene applied to the surface of the electrode acts as a modifying agent, which allows to

reduce the resistance at the electrode/electrolyte interface [4]. The promise of graphene-related technologies is confirmed by the Applied Market Research findings, according to which the global lithium-ion battery market with graphene use will reach $95.6 billion by 2027.

The improvement of the electrochemical characteristics of $LiMn_2O_4$/graphene composite electrodes is achieved by the optimization of the $LiMn_2O_4$ synthesis method [8-10], the selection of graphene with suitable physico-chemical parameters and the optimization of the graphene/$LiMn_2O_4$ composite electrodes manufacturing technology. The specific capacity of $LiMn_2O_4$/graphene composite electrodes and their stability during cycling is also determined by the physico-chemical properties of spinel itself, such as structure, surface morphology, particle sizes and the presence of impurities.

A simple sol-gel method for the synthesis of nanoparticles $LiMn_2O_4$ with farther creation of $LiMn_2O_4$/graphene composite proposed in Ref. [8]. The initial specific capacities of bare $LiMn_2O_4$ and $LiMn_2O_4$/graphene composite electrodes were 127 mAh/g and 135 mAh/g, respectively, and after 100 cycles at 1 C decreased to 109.9 and 115.6 mAh/g. A noticeable improvement was also achieved during rate tests. The obtained high specific characteristics at significant discharge currents are explained by the increased electronic conductivity of composite electrodes. The production of graphene/$LiMn_2O_4$ composite electrodes by the method of hydrothermal synthesis is considered in Refs. [9, 10]. Nanoparticles of $LiMn_2O_4$ optimally distributed in the graphene matrix of the electrode contribute to an increase in the rate of charge transfer, which provides electrodes with a high capacity at high current density. In addition, graphene particles on the surface of $LiMn_2O_4$ reduce the negative influence of the Jahn–Teller effect, which ensures the stability of the specific capacity during long-term cycling. The positive effect of the presence of graphene in the composition of composite electrodes, which is achieved due to the combination of the structure and morphology of the electrode material and graphene, is considered in publications [11-17].

Composite electrodes $LiMn_2O_4$/graphene and $LiCr_{0.1}Mn_{1.95}O_4$/graphene had a specific capacity of 130 and 140 mAh/g at a current density of 0.1 C that are higher than for graphene-free samples. Also, higher specific capacities were obtained at a current density of 8 C, which were 48 and 70 mAh/g, respectively [11]. In addition, graphene composites were made without binder adding as a self□standing electrode, where spinel nanorods were homogenously embedded between graphene layers providing better electron transport of electrodes. Enhanced cycling and rate performances were obtained in a case of $LiMn_2O_4$ and 3D graphene composite [12]. The specific capacity of the composite was 133 and 90 mAh/g at current rates of 0.5 C and 10 C, respectively. This was the result of the improved electronic conductivity and lithium ions diffusion rate caused by the high surface area and rich three-dimensional porous channels of graphene. Composite electrodes made of graphene sheets and $LiMn_2O_4$ particles modified with Y_2O_3 had increased electronic conductivity due to the uniform distribution of spinel particles in the electrode structure and the Y_2O_3 surface modification also reduced the solubility of Mn^{3+} [15]. This made it possible to obtain the excellent capacity retention at an elevated temperature 55 °C (89.3 % after 500 cycles at a rate of 1 C) and high rate performance with capacity of 90.0 mAh/g at 30 C.

The presence of graphene in the composition of electrodes has a positive effect in the case of other electrode materials as well. The authors [16, 17] showed an increase in cycling stability and rate characteristics of $LiFePO_4$ in graphene presence, which is associated with providing abundant porous channels for the diffusion of lithium ions and creation of graphene conducting network for easy charge transfer. In the case of composite of NMC-type cathode materials with different graphenes (graphene oxide), their common advantages are higher electronic conductivity and better interfacial charge transfer process. [18-21]. In addition, graphene performs a protective function slowing the cathode/electrolyte interfacial side reaction both in the system with liquid electrolyte [20] and in the all-solid-state system [21]. The authors

[19] showed that graphene also ensures the mechanical integrity of the NMC electrode by restraining the propagation of microcracks. The same advantages of using graphene materials are characteristic of anodic composites, for example based on TiO_2 [22-25].

In this work, the electrochemical characteristics of composite electrodes based on spinel $LiMn_2O_4$ with commercial samples of graphene nanoplatelets were investigated. The influence of structural, morphological and surface characteristics of $LiMn_2O_4$ and graphenes on the capacitive and kinetic characteristics of composite electrodes based on them is shown. The role of graphene in achieving high electrochemical characteristics is determined.

Experimental

Commercial graphene produced by XG Sciences Inc. (USA) was used in the work [26]. The graphene samples used are marked xGnP 50-80, xGnP 300 and xGnP 750, where the numbers correspond to the specific surface area declared by the manufacturer. As the active material of the cathode were taken samples of lithium-manganese spinel $LiMn_2O_4$, which were synthesized by a solid-state synthesis method and by means of a citric acid-aided route. Solid-state synthesis of $LiMn_2O_4$ was performed from the mixture of lithium carbonate and manganese carbonate, which was first pyrolyzed at temperature of 450 □ for 6 h and then annealed for 12 h at temperature of 750 □. For citric acid aided syntheses, citrate precursors were obtained from a mixture of $LiNO_3$, $Mn(NO_3)_2$ and $C_6H_8O_7$ solutions (all reagents are analytical grade from Makrokhim, Ukraine) according to the procedure described in Refs. [27, 28]. The precursor obtained in this way was subjected to pyrolysis at 400 °C for 4 h and then the products obtained were annealed at 750 °C for 12 h. Farther in the text, $LiMn_2O_4$ samples synthesized by solid-state and citrate methods are marked LMO-SS and LMO-Citrate, respectively.

X-ray diffraction (XRD) measurements of graphene and $LiMn_2O_4$ samples were carried out using a DRON 4-07 (LOMO, Russia) diffractometer with a Cu-Ka (λ = 0.154 nm) radiation and a registration step of 0.05 degrees (2θ). The morphology of materials was investigated using a JSM-6700F (JEOL, Japan) scanning electron microscope (SEM). Porosity studies were carried out on a ASAP 2000 (Micromeritics, USA) device.

Electrochemical measurements were performed in CR2016 coin cells with lithium metal anode. The electrodes consisted of 80 % of $LiMn_2O_4$, 5 % of graphene, 5 % of Super C65 carbon black (Imerys Graphite and Carbon, Belgium) and 10 % of a polyvinylidene fluoride binder Solef 6020 (Solvay, Belgium). The active material, graphene and carbon black were added to solution of PVDF in dimethylacetamide and dispersed to form a slurry. The resulting slurry was coated on an aluminum foil using a doctor blade applicator and then dried at a temperature of ~70 □ until the solvent was completely removed. After the farther compaction the discs with a surface area of 2 cm^2 were cut from the resulting tape. Before cell assembling, the electrode discs were dried at 120 □ in a vacuum. A Celgard 2400 film was used as a separator. The electrolyte was a 1 M solution of lithium hexafluorophosphate $LiPF_6$ (Gelon, China) in a mixture of ethylene carbonate (EC, 98%, Aldrich) and dimethyl carbonate (DMC, 99%, Aldrich) solvents in a volume ratio of 1:1. All operations on the production of electrolytes, their storage and assembly of elements were carried out in dry glove boxes with an argon atmosphere.

The charge/discharge testing of the cells was performed on a Battery Testing System (Neware, China) battery tester in the voltage range of 3-4.4 V. The cycling currents were expressed in C units, which were calculated based on the value of the theoretical specific capacity of $LiMn_2O_4$ of 148 mAh/g (1 C = 148 mA/g). Electrochemical impedance spectroscopy (EIS) measurements were performed in the frequency range 50 kHz – 0.1 Hz and applied voltage amplitude of 10 mV. The resulting impedance dependences were analyzed using ZView software.

Results and Discussion

Physico-chemical characterization of xGnP graphene nanoplatelets

The structural, surface and morphological properties of graphene are decisive for their effective use as part of the electrode composites of lithium-ion batteries. In view of this, we investigated some important physico-chemical characteristics of graphene that were missing from the certificates provided by the supplier or published in open literature sources. Fig. 1 presents XRD patterns of graphene samples, which show that the intensity of the peaks decreases in the range of xGnP 50-80, xGnP 300 and xGnP 750. This is a consequence of the difference in the crystal structure of graphene, namely the orderliness of the graphene structure, crystallite sizes, and the number of layers in them. The main (002) peak at ~ 26.5° corresponds to the distance between the graphene layers. The calculated values of the interplanar distance $d_{(002)}$ are presented in Table. 1. The given $d_{(002)}$ values are very close for all investigated graphene samples. The crystallite sizes $L_{(002)}$ calculated from the width of the same peak are close for the xGnP 50-80 and xGnP 300 samples and actually three times smaller for the xGnP750 graphene. The approximate number of layers calculated from the $L_{(002)}/d_{(002)}$ ratio ranges from 14 for xGnP 750 graphene to 46 for xGnP 50-80 and xGnP 300 graphenes.

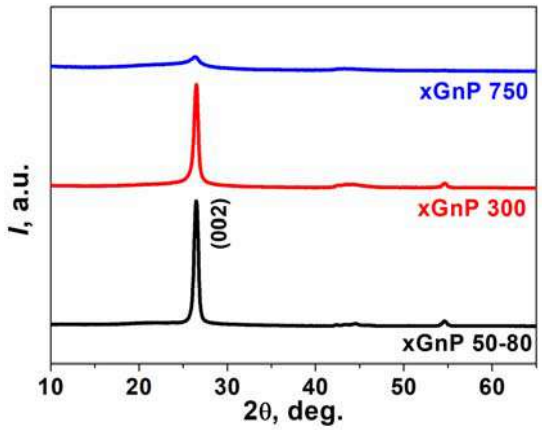

Fig.1. XRD patterns of graphene samples.

Table 1. Structural parameters of graphene samples calculated from XRD data.

Graphene sample	2θ (002), deg.	Interplanar distance $d_{(002)}$, Å	Crystallite size $L_{(002)}$, nm	Number of layers
xGnP 50-80	26.47	3.37	15.3	45.4
xGnP 300	26.46	3.37	15.4	45.7
xGnP750	26.36	3.38	4.8	14.1

The main differences between graphene samples lie in their morphological and surface properties. Fig. 2 presents SEM micrographs of graphenes at different magnifications. According to the micrographs, the graphene samples consist of particles up to 5 μm in size for the xGnP 50-80 sample and up to 2 μm for the xGnP 300 and xGnP 750 samples, formed from stacks of graphene layers of the thickness up to 15 nm, according to XRD data, which is consistent with the manufacturer's data. For xGnP 50-80 graphene, the size (diameter) of the platelets coincides with the size of the particles, which are characterized by loose packing. In the case of xGnP 300 and xGnP750 samples, the sizes of stacks of graphene layers that form individual particles decrease and the structure of these graphenes is denser, while having larger surface area and porosity as shown in Fig. 3 and Table. 2. The obtained values of the specific surface area $S_{sp.}$ are 44, 309 and 789 m^2/g for xGnP 50-80, xGnP 300 and xGnP 750, respectively, that is close to those declared by the manufacturer. Graphene xGnP 50-80 has low porosity, which is determined mostly by the presence of macropores and relatively small amount of mesopores with the radius of 1.9 nm makes little difference to the overall porosity. Graphenes xGnP 300 and

xGnP 750 have a sufficiently developed mesoporous structure with a bimodal distribution of pores with average radii of 1.8-1.9 and 6.3-6.5 nm.

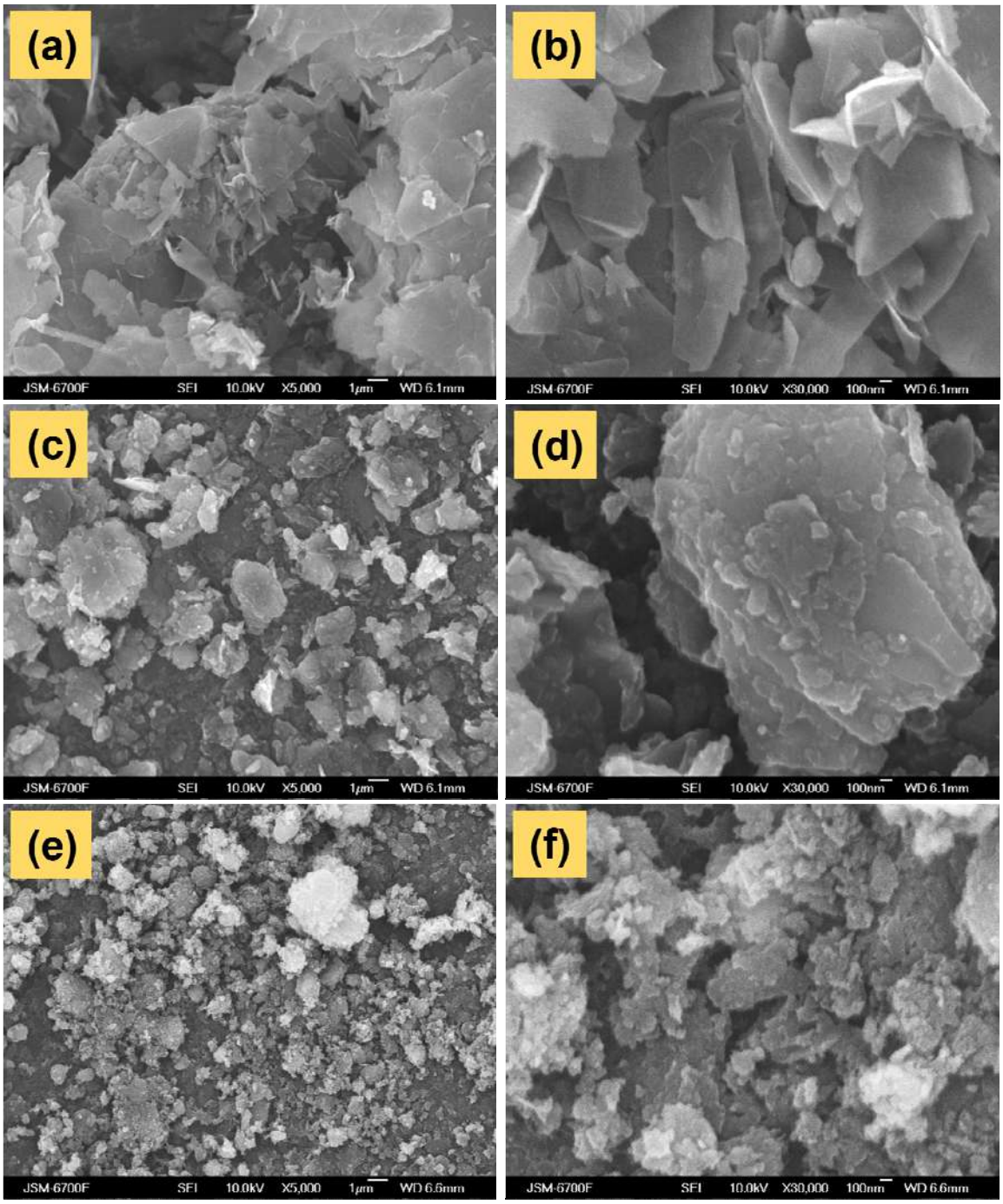

Fig. 2. SEM of graphene samples (a, b) xGnP 50-80, (c, d) xGnP 300 and (e, f) xGnP 750.

Differences in the morphological and surface characteristics of graphene allow us to assume their influence on the formation of the macrostructure of the electrode, which affects the kinetics of electronic and ionic transport [29]. $LiMn_2O_4$ spinel belong to materials with relatively low electronic conductivity, which is approximately $0.28\text{-}2.2\times10^{-6}$ S/cm [30], therefore a conductive additive is necessary for their effective operation. But the contact in the active electrode material-conductive additive system is a derivative of their morphological features. The properties of electrically conductive additives (including graphene) determine the magnitude of not only electronic, but also ionic charge transfer. Graphene is able to change the porosity of

the electrode and, as a result, affect the rate of lithium ion transfer due to migration and convection processes [31]. From this point of view, the morphology and structure of graphene is a very important factor affecting the specific and kinetic characteristics of electrodes. It is known that the difference in particle size between graphene and cathode active material affects the characteristics of the transport path and as a resalts changes the rate of Li^+ diffusion. Therefore, when choosing graphene, it is extremely important to take into account the ratio of the particle sizes of graphene and active material used, which as a result allows optimizing the balance of electronic and ionic charge transfer in electrode volume [32].

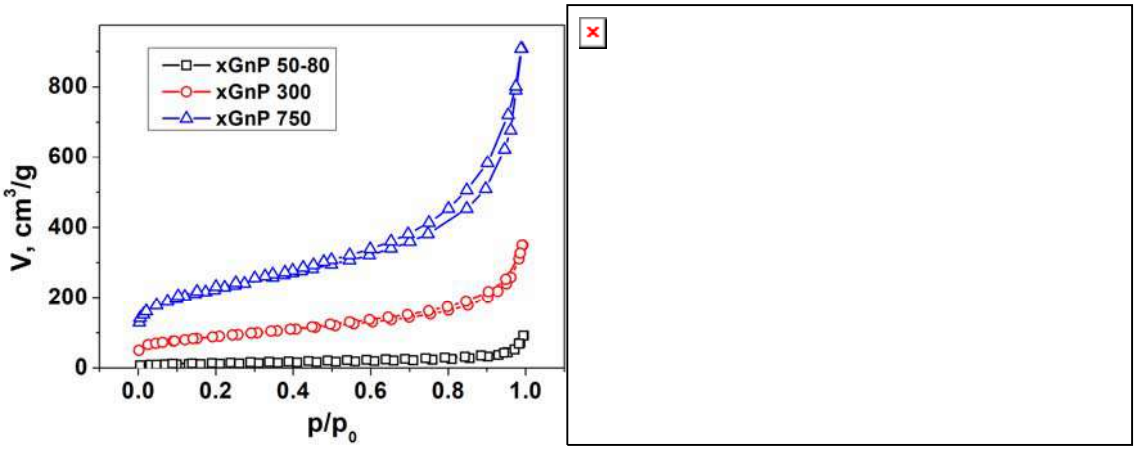

Fig. 3. Nitrogen adsorption/desorption isotherms and pore distribution curves for graphene samples.

Table 2. Surface characteristics of graphene samples.

Graphene sample	Specific surface area S_{sp}, m^2/g	Pore volume V_{pore}, cm^3/g	Pore radius r_{pore} (BJH), nm
xGnP 50-80	44	0.142	1.9
xGnP 300	309	0.542	1.9; 6.5
xGnP 750	789	1.408	1.8; 6.3

Physico-chemical characterization of $LiMn_2O_4$ samples

The use of different synthesis methods leads to differences in the structural and morphological characteristics of the materials and largely determines their behavior as active electrode materials. Lithium-manganese spinels are no exception, so the synthesized materials were investigated by the XRD and SEM methods. Presented in Fig. 4 diffractograms testify to the formation in both cases of crystalline $LiMn_2O_4$ with a characteristic cubic structure (space group *Fd3m*), which is indicated by the presence of intense reflections from the crystal planes (111), (311), (222), (400), (331), (511), (440) and (531). In addition to the main phase, in the case of citrate $LiMn_2O_4$, there is a weak impurity peak of unlithiated phase of Mn_3O_4. Presented in Table. 3 structural parameters of $LiMn_2O_4$ do not differ much and are in good agreement with literature data [33]. Despite the similarity in structural parameters, the used $LiMn_2O_4$ samples are characterized by significant differences in morphology, as shown in Fig. 5. It is clear from the presented micrographs that the synthesis method significantly affects the size of $LiMn_2O_4$ particles. In both cases $LiMn_2O_4$ samples consist of practically non-agglomerated particles. In the case of solid-state synthesis, the particle sizes of the spinel are 200-500 nm and for citrate spinel are 100-200 nm. The citric acid aided synthesis method provides smaller particle sizes and narrower distribution of particles than the solid-state method.

Fig. 4. XRD patterns of $LiMn_2O_4$ samples.

Table 3. Structural parameters of $LiMn_2O_4$ samples.

Spinel sample	Lattice parameter, Å	Lattice volume, $Å^3$	Crystallite size $D_{(400)}$, nm
Solid-state	8.241	560	28
Citrate	8.241	560	22

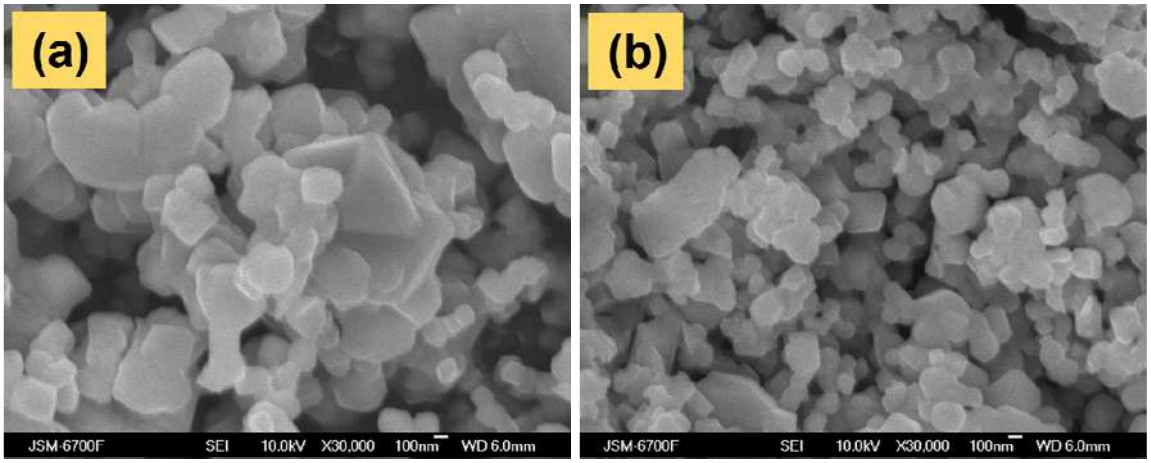

Fig. 5. SEM micrographs of $LiMn_2O_4$ synthesized by (a) solid-state and (b) citric acid aided methods.

Electrochemical properties of $LiMn_2O_4$/graphene composites

Fig. 6 and 7 show the charge/discharge curves and the corresponding differential capacity curves obtained during discharge current densities of 0.5 C, 10 C, and 20 C and constant charge current of 0.5 C, respectively, for LMO-Citrate and LMO-SS with different graphenes. Their character is typical for the deintercalation/intercalation of lithium ions in the spinel structure, which can be expressed as follow

$$LiMn_2O_4 \leftrightarrow Li_{1-x}Mn_2O_4 + xLi^+ + xe^-.$$

Two plateaus on the charge/discharge curves correspond to two peaks on the differential curves, reflecting a reversible two-stage phase transformation $LiMn_2O_4 \leftrightarrow Li_{0.5}Mn_2O_4 \leftrightarrow \lambda$-$MnO_2$. In all cases of LMO/graphene combinations the discharge curves at a current density of 0.5 C have similar average voltages on the plateaus (peak positions on the differential curves), which are 4.02 and 4.13 V on charge and 3.98 and 4.105 V on discharge, respectively. The difference in voltages between the corresponding charge and discharge peaks is 40 and 25 mV for the first and second peaks, respectively. Small differences in the voltage of the discharge and charge process indicate the low polarization and high reversibility of these processes at the low

current load. At current density of 0.5 C, the specific capacity of LMO-Citrate spinel is practically independent of the graphene sample and is 97, 99 and 90 mAh/g for electrodes with xGnP 50-80, xGnP 300 and xGnP 750, respectively. The type of graphene also does not significantly affect the specific capacity of LMO-SS spinel. At the current density of 0.5 C, its specific capacity is 114 mAh/g for electrodes with xGnP 50-80 and xGnP 750 graphenes and 119 mAh/g in a case of xGnP 300 graphene. An increase in the discharge current to 10 and 20 C leads to a polarization of the discharge curves, which is smaller in the case of composites with spinel LMO-Citrate. This indicates better kinetic characteristics of LMO-Citrate spinel compared to LMO-SS regardless of the graphene sample. These changes are even better visible on the cathodic branches of the corresponding differential curves, where two peaks are still clearly visible for the LMO-Citrate/graphene composites at a current of 10 C, in contrast to the LMO-SS/graphene composites. At the current density of 20 C, the specific capacity of $LiMn_2O_4$-Citrate spinel with xGnP 50-80 and xGnP 300 graphenes decreases to 48 mAh/g and in a case of xGnP 750 graphene to 40 mAh/g. The specific capacity of LMO-SS spinel at the same current density is much lower and is 20, 27 and 25 mAh/g for composites with xGnP 50-80, xGnP 300 and xGnP 750 graphenes, respectively.

The dependences of specific capacity on cycle number at different current densities is shown in Fig. 8. For all composite electrodes, a relatively low discharge specific capacity was obtained in the first cycle, which gradually rises to a constant value by the 5th cycle. For LMO-Citrate spinel, the discharge capacity increases from 86 to 96 mAh/g, from 83 to 98 mAh/g, and from 78 to 89 mAh/g for composites with xGnP 50-80, xGnP 300, and xGnP 750 graphenes, respectively. Along with the capacity, the coulombic efficiency (CE) of the first cycle is low, which is 81, 75, and 79 % for xGnP 50-80, xGnP 300, and xGnP 750 graphenes, respectively. However, by the 5th cycle CE stabilizes at the level of 98-99 % for all compositions of the composite. Similar dynamics of changes in specific capacity and CE were obtained in the case of graphene composites based on LMO-SS spinel. From the first to the fifth cycle, the capacity increases from 97 to 113 mAh/g, from 118 to 119 mAh/g, and from 100 to 112 mAh/g for composites with xGnP 50-80, xGnP 300, and xGnP 750 graphenes, respectively. The corresponding values of CE of the first cycle are 82, 90 and 85 %. Reduced CE and low capacity of the first cycles can be associated with a significant share of side processes, the formation of a stable solid electrolyte interface (SEI), as well as insufficient development of the entire electrode volume. The further change of the specific capacity at different discharge currents is determined by the nature of the spinel itself and depends to a lesser extent on the graphene sample in the composite. The differences obtained within the same spinel with different graphenes are not large. After removal of the current load and return to discharge with a current of 0.5 C for composites with both spinels, the specific capacity is not fully restored. Thus, the capacity retention at 70 cycles (including discharge with currents up to 20 C) is higher for LMO-Citrate/graphene composites, being 91, 90, and 92 % with xGnP 50-80, xGnP 300, and xGnP 750 graphenes, respectively. For LMO-SS spinel composites with xGnP 50-80, xGnP 300, and xGnP 750 graphenes, similar values are 87, 86, and 88 %, respectively. This manifests the better cyclability and rate capability of LMO-Citrate spinel compared to LMO-SS.

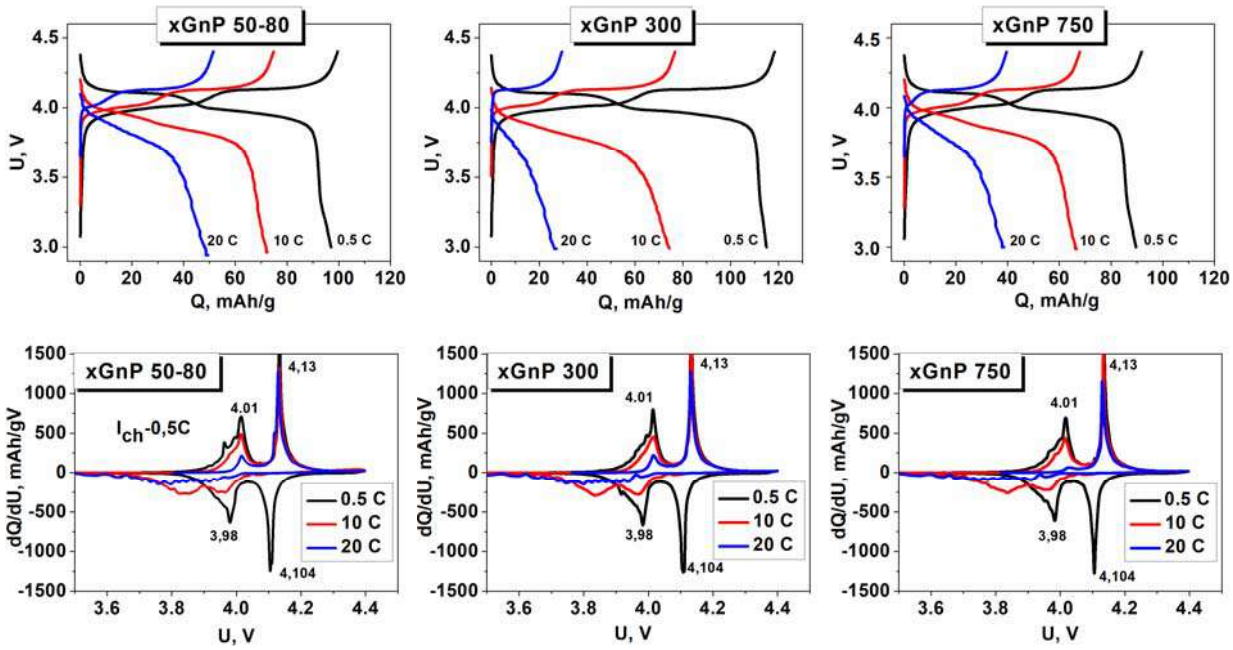

Fig. 6. Charge/discharge curves and the corresponding differential capacity curves at different discharge current densities (constant charge current density of 0.5 C) for LMO-Citrate/graphene composites.

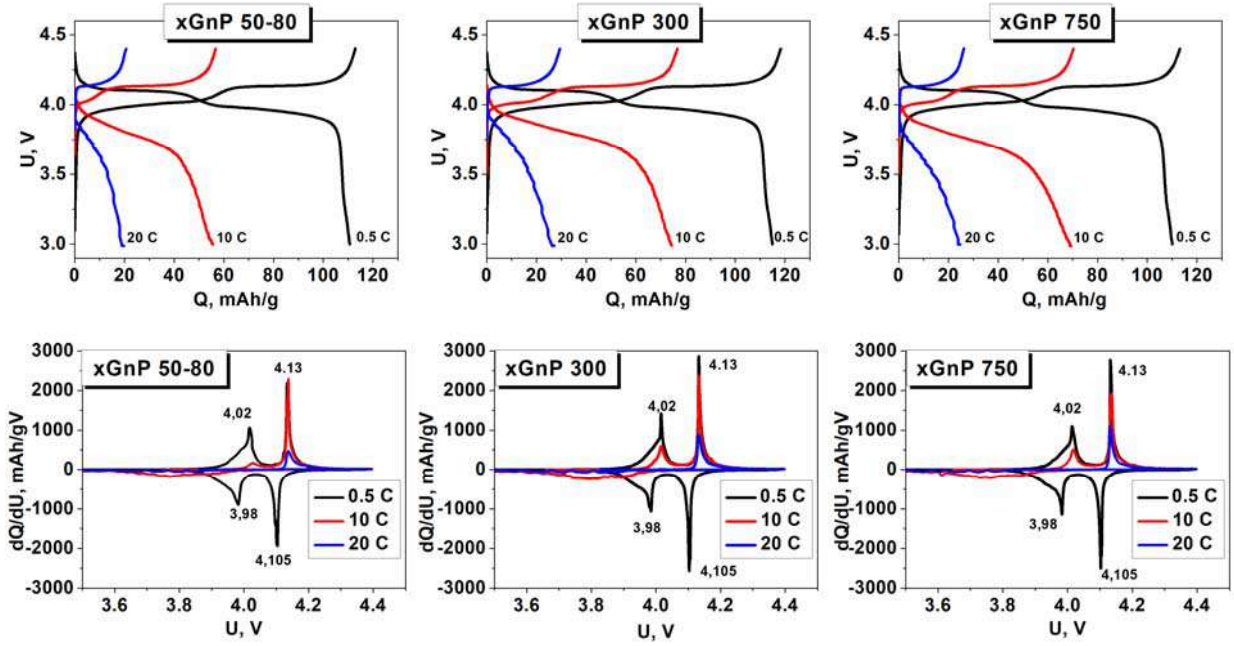

Fig. 7. Charge/discharge curves and the corresponding differential capacity curves at different discharge current densities (constant charge current density of 0.5 C) for LMO-SS/graphene composites.

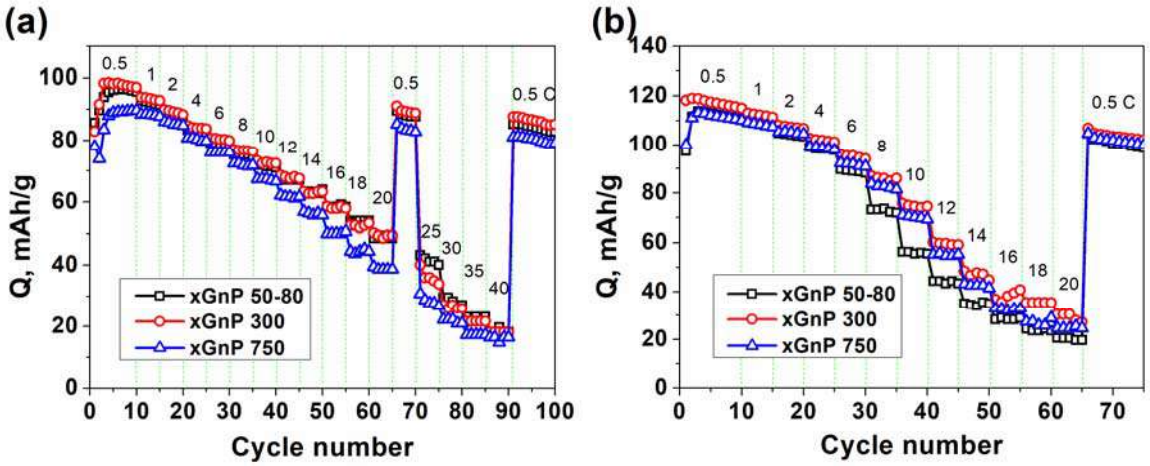

Fig. 8. Cycling performance of graphene composites with (a) LMO-Citrate and (b) LMO-SS spinels.

The dependences of specific capacity on discharge current density are shown in Fig. 9. The capacity of each of the samples obtained at a current of 0.5 C was taken as 100 %. LMO-SS/graphene composites are characterized by a faster decrease in specific capacity per unit increase in current density than LMO-Citrate/graphene composites. Thus, the capacity retention of ~20 % is achieved at current density of 40 C for LMO-Citrate and at 20 C in a case LMO-SS composites. The speed characteristics of the electrodes can be estimated by the ratio of the change in specific capacity per unit of discharge current $dQ/dI = (Q_{max} - Q_{min}) / (I_{max} - I_{min})$, where Q_{max} and Q_{min} are discharge capacity at minimum and maximum discharge rate in C unit, respectively [34]. The calculations were carried out for the same range of discharge currents from 0.5 to 20 C. For LMO-Citrate spinel, the dQ/dI values are 2.42, 2.45, and 2.62 in the case of composites with xGnP 50-80, xGnP 300, and xGnP 750 graphenes, respectively. In the case of LMO-SS spinel, the same values are larger and are 4.67, 4.51, and 3.89, respectively, for composites with xGnP 50-80, xGnP 300, and xGnP 750 graphenes. Thus, LMO-Citrate spinel has a significantly higher resistance to discharge at high current densities. The obtained results show a significant influence of the nature of spinel on the speed characteristics of the electrodes. At the same time, the type of graphene has no significant effect on the value of dQ/dI.

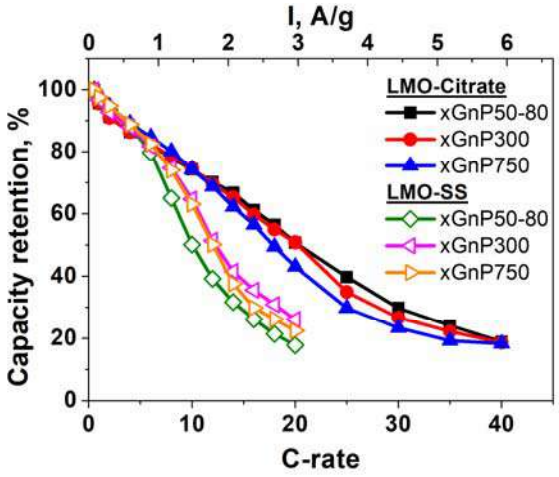

Fig. 9. Capacity retention of $LiMn_2O_4$ in composites with different graphenes.

The kinetic characteristics of composite electrodes were assessed based on the electrochemical impedance spectra obtained before cycling and after 70 cycles. The Nyquist plots presented in Fig. 10 have a typical form and composed of a semicircle in the high frequency and a quasi-straight line in the low frequency. The high frequency intercept of Z' is

assigned to the ohmic resistance or electrolyte resistance (R_{el}). The medium-frequency intercept (resistance of semicircle) is attributed to the charge transfer resistance (R_{ct}) and reflects lithium-ion migration through the SEI and charge transfer between the electrolyte and electrode interface. The low-frequency region represents the lithium ion diffusion in solid phase. All obtained impedance spectra are sufficiently close to each other regardless of the composition. A common feature of composites with LMO-Citrate and LMO-SS is a decrease in the respective resistances after cycling compared to the initial values. The results of fitting of electrochemical impedance spectroscopy are shown in Tables 4 and 5.

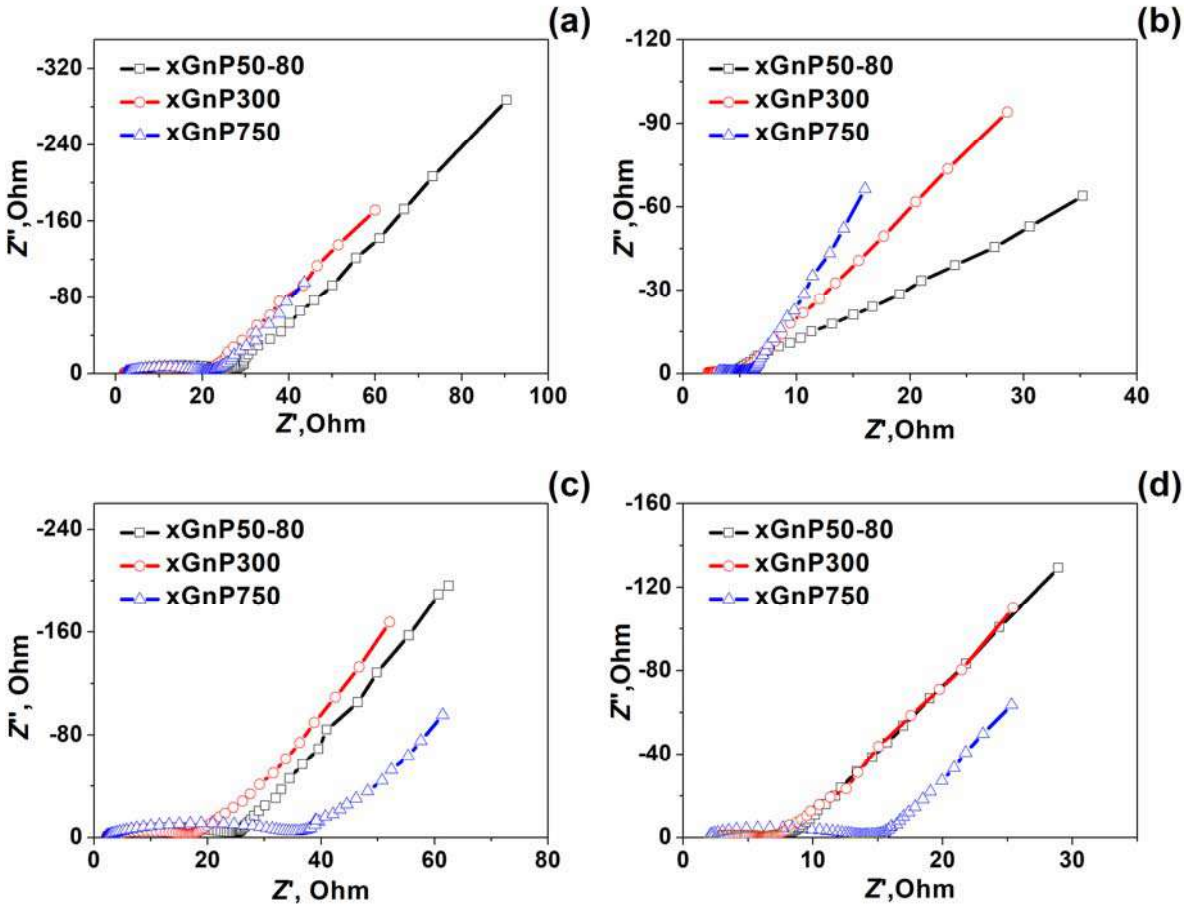

Fig. 10. Nyquist plots of the composites electrodes (a) LMO-Citrate/graphene before cycling, (b) LMO-Citrate/graphene after 70 cycles, (c) LMO-SS/graphene before cycling and (d) LMO-SS/graphene after 70 cycles.

The value of R_{ct} can be used to calculate the exchange current (i_0), which characterizes the reversibility of the electrochemical process. The exchange current density i_0 can be calculated according to following Eq. [35]

$$i_0 = RT/nFR_{ct}\,.$$

where R is the gas constant, T is the absolute temperature, n is the number of transferred electrons, F is Faraday constant, and R_{ct} is charge transfer resistance.

The obtained values of the i_0 before cycling are close enough and practically does not depend on the composition of the electrode. After 70 cycles, an increase of i_0 is observed, and the magnitude of which depends on both spinel and graphene. Depending on the graphene sample, the i_0 values for composites with LMO-Citrate spinel increases by almost an order of magnitude. An increase of the i_0 for composites with LMO-SS is significantly smaller being up to 2.5 times. The electrode reaction with higher exchange current is easier to carry out and has

greater reversibility, which corresponds to better electrochemical performance [36, 37]. Based on this, the values of the exchange currents before cycling do not fully reflect the future electrochemical behavior of the composites, while the corresponding values after 70 cycles are consistent with the demonstrated electrochemical characteristics. The calculated values of the distributed capacity C_0 that characterize the surface properties (the double layer capacitance) of electrodes after cycling in most cases decrease with the exception of LMO-Citrate spinel composites with xGnP 50-80 and xGnP 300 graphenes. The decrease in C_0 depends on the type of graphene and may be the result of a change in surface properties of electrodes and reducing the number of charge carriers at the electrode-electrolyte interface.

Table 4. Fitting results of electrochemical impendance spectroscopy for LMO-Citrate/graphene composites

Graphene sample	Before cycling			After 70 cycles		
	Contact resistance R_{ct}, Ohm	Exchange current i_0, A/cm^2	Capacity C_0, F/cm^2	Contact resistance R_{ct}, Ohm	Exchange current i_0, A/cm^2	Capacity C_0, F/cm^2
xGnP 50-80	26.84	1.91×10^{-3}	4.27×10^{-6}	2.38	2.13×10^{-2}	2.2×10^{-5}
xGnP 300	19.74	2.59×10^{-3}	4.39×10^{-6}	3.04	1.7×10^{-2}	1.45×10^{-5}
xGnP 750	19.93	2.57×10^{-3}	4.3×10^{-6}	3.26	1.57×10^{-2}	1.7×10^{-6}

Table 5. Fitting results of electrochemical impendance spectroscopy for LMO-SS/graphene composites

Graphene sample	Before cycling			After 70 cycles		
	Contact resistance R_{ct}, Ohm	Exchange current i_0, A/cm^2	Capacity C_0, F/cm^2	Contact resistance R_{ct}, Ohm	Exchange current i_0, A/cm^2	Capacity C_0, F/cm^2
xGnP 50-80	24.36	2.1×10^{-3}	4.96×10^{-6}	8.6	2.97×10^{-3}	2.06×10^{-6}
xGnP 300	16.71	3.06×10^{-3}	4.97×10^{-6}	6.66	7.68×10^{-3}	0.7×10^{-6}
xGnP 750	35.59	1.43×10^{-3}	5.36×10^{-6}	14.33	3.58×10^{-3}	0.8×10^{-6}

Conclusions

In summary, a study of composite electrodes based on $LiMn_2O_4$ containing commercial graphene nanoplatelets was conducted. Using the solid-state and citric acid aided synthesis methods, the $LiMn_2O_4$ samples with different structural and morphological characteristics were obtained, which were used as the active material. The used industrial graphene samples had a nanoplatelets morphology with particle sizes up to 5 μm and different specific surface areas (44, 309 and 789 m^2/g). The combination of $LiMn_2O_4$ and graphenes with different particle sizes and morphologies made it possible to obtain electrodes that demonstrated high electrochemical characteristics due to the creation an electrode structure with high charge transfer properties. Electrochemical studies have shown a significant influence of the nature of $LiMn_2O_4$ on the cycling stability and rate capability. At the same time, the influence of graphene type within one spinel was relatively small. Despite the lower initial specific capacity, LMO-Citrate/graphene composites demonstrated better cycling stability and higher maximum discharge currents up to 40 C compared to LMO-SS/graphene composites. The results of electrochemical impedance spectroscopy are in good agreement with the results of cyclic tests and confirm the high kinetic characteristics of LMO/graphene composites.

References

1. Ramos Ferrer P., Mace A., Thomas S.N., Jeon J.W. Nanostructured porous graphene and its composites for energy storage applications. *Nano Converg*. 2017. **4**: 1.

2. Zhu S., Sheng J., Chen Y., Ni J., Li Y. Carbon nanotubes for flexible batteries: recent progress and future perspective. *Natl. Sci. Rev*. 2021. **8**(5): 1.
3. Ahmad Y., Colin M., Gervillie-Mouravieff C., Dubois M., Guérin K. Carbon in lithium-ion and post-lithium-ion batteries: recent features. *Synth. Met*. 2021. **280**: 116864.
4. Cai X., Lai L., Shen Z., Lin J. Graphene and graphene-based composites as Li-ion battery electrode materials and their application in full cells. *Journal of Materials Chemistry A*. 2017. **5**: 15423.
5. Yang S., Sun Y., Chen L., Hernandez Y., Feng X., Müllen K. Porous iron oxide ribbons grown on graphene for high-performance lithium storage. *Sci. Rep*. 2012. **2**(1): 1.
6. Lin J., Raji A.R.O., Nan K., Peng Z., Yan Z., Samuel E.L., Natelson D., Tour J.M. Iron oxide nanoparticle and graphene nanoribbon composite as an anode material for high-performance Li-ion batteries. *Adv. Funct. Mater.* 2014. 24(14): 2044.
7. Prabakar S.R., Hwang Y.H., Lee B., Sohn K.S., Pyo M. Graphene-sandwiched $LiNi_{0.5}Mn_{1.5}O_4$ cathode composites for enhanced high voltage performance in Li ion batteries. *J. Electrochem. Soc*. 2013. **160**(6): A832.
8. Aziz S., Zhao J., Cain C., Wang Y. Nanoarchitectured $LiMn_2O_4$/graphene/ZnO composites as electrodes for lithium ion batteries. *J. Mater. Sci. Technol*. 2014. **30**(5): 427.
9. Lin B., Yin Q., Hu H., Lu F., Xia H. $LiMn_2O_4$ nanoparticles anchored on graphene nanosheets as high-performance cathode material for lithium-ion batteries. *J. Solid State Chem*. 2014. **209**: 23.
10. Pyun M.H., Park Y.J. Graphene/$LiMn_2O_4$ nanocomposites for enhanced lithium ion batteries with high rate capability. *J. Alloys Compd*. 2015. **643**: S90.
11. Guler A., Duman S.O., Nalci D., Guzeler M., Bulut E., Guler M.O., Akbulut H. Graphene assisted template based $LiMn_2O_4$ flexible cathode electrodes. *Int. J. Energy Res*. 2018. **42**(9): 2971.
12. Luo X.D., Yin Y.Z., Yuan M., Zeng W., Lin G., Huang B., Li Y.W., Xiao S.H. High performance composites of spinel $LiMn_2O_4$/3DG for lithium ion batteries. *RSC Adv*. 2018. **8**(2): 877.
13. Jaber-Ansari L., Puntambekar K.P., Kim S., Aykol M., Luo L., Wu J., Myers B.D., Iddir H., Russel J.T., Saldaña S.J., Kumar R., Thackeray M.M., Curtiss L.A., Dravid V.P., Wolverton C., Hersam M.C. Suppressing manganese dissolution from lithium manganese oxide spinel cathodes with single-layer graphene. *Adv. Energy Mater*. 2015. **5**(17): 1500646.
14. Ilango P.R., Prasanna K., Subburaj T., Jo Y.N., Lee C.W. Facile longitudinal unzipping of carbon nanotubes to graphene nanoribbons and their effects on $LiMn_2O_4$ cathodes in rechargeable lithium-ion batteries. *Acta Mater*. 2015. **100**: 11.
15. Ju B., Wang X., Wu C., Yang X., Shu H., Bai Y., Wen W., Yi X. Electrochemical performance of the graphene/Y_2O_3/$LiMn_2O_4$ hybrid as cathode for lithium-ion battery. *J. Alloys Compd*. 2014. **584**: 454.
16. Ha J., Park S.K., Yu S.H., Jin A., Jang B., Bong S., Kim I., Sung Y.E., Piao Y. A chemically activated graphene-encapsulated $LiFePO_4$ composite for high-performance lithium ion batteries. *Nanoscale*. 2013. **5**(18): 8647.

17. Dutta D., Santhosha A.L., Sood A.K., Bhattacharyya A.J. Reducing Li-diffusion pathways via “adherence” of ultra-small nanocrystals of $LiFePO_4$ on few-layer nanoporous holey-graphene sheets for achieving high rate capability. *RSC Adv*. 2016. **6**(92): 89328.

18. Guler A., Gungor H., Ozcan S., Coban A., Guler M.O., Akbulut H. A high-performance composite positive electrode based on graphene and $Li(Ni_{1/3}Co_{1/3}Mn_{1/3})O_2$. *Int. J. Energy Res*. 2018. **42**(14): 4499.
19. Alqahtani Y.M., Williams Q.L. Reduction of capacity fading in high-voltage NMC batteries with the addition of reduced graphene oxide. *Materials*. 2022. **15**(6): 2146.
20. Wu F., Yan Y., Wang R., Cai H., Tong W., Tang H. Synthesis of $LiNi_{1/3}Mn_{1/3}Co_{1/3}O_2$@graphene for lithium-ion batteries via self-assembled polyelectrolyte layers. *Ceram. Int*. 2017. **43**(10): 7668.
21. Zhuang Z., Yang L., Ju B., Yin A., Lei G., Zhou Q., Tang Y., Deng Z., Tu F., Qin S. Engineering $LiNi_{0.5}Co_{0.2}Mn_{0.3}O_2$/poly(propylene carbonate) interface by graphene oxide modification for all-solid-state lithium batteries. *Energy Storage*. 2020. **2**(2): e109.

22. Du T., Zhang W., Peng H., Jain G. Mesoporous TiO_2 spheres/graphene composite as a high-performance anode material for lithium-ion batteries. *Int. J. Electrochem. Sci*. 2018. **13**: 6229.
23. Farooq U., Ahmed F., Pervez S.A., Rehman S., Pope M.A., Fichtner M., Roberts E.P. A stable TiO_2–graphene nanocomposite anode with high rate capability for lithium-ion batteries. *RSC Adv*. 2020. **10**(50): 29975.
24. Jamal H., Kang B.S., Lee H., Yu J.S., Lee C.S. Comparative studies of electrochemical performance and characterization of TiO_2/graphene nanocomposites as anode materials for Li-secondary batteries. *J. Ind. Eng. Chem*. 2018. **64**: 151.
25. Zhang X., Suresh Kumar P., Aravindan V., Liu H.H., Sundaramurthy J., Mhaisalkar S.G., Duong H.M., Ramakrishna S., Madhavi S. Electrospun TiO_2–graphene composite nanofibers as a highly durable insertion anode for lithium ion batteries. *J. Phys. Chem. C*. 2012. **116**(28): 14780.
26. XG Sciences - Products. https://xgsciences.us/aboutxgnp.html.
27. Farbun I.A., Romanova I.V., Kirillov S.A. Optimal design of powdered nanosized oxides of high surface area and porosity using a citric acid aided route, with special reference to ZnO. *J. Sol-Gel Sci. Technol*. 2013. **68**(3): 411.
28. Potapenko A.V., Chernukhin S.I., Romanova I.V., Rabadanov K.S., Gafurov M.M., Kirillov S.A. Citric acid aided synthesis, characterization, and high-rate electrochemical performance of $LiNi_{0.5}Mn_{1.5}O_4$. *Electrochim. Acta*. 2014. **134**: 442.
29. Park M., Zhang X., Chung M., Less G.B., Sastry A.M. A review of conduction phenomena in Li-ion batteries. *J. Power Sources*. 2010. **195**(24): 7904.
30. Marzec J., Świerczek K., Przewoźnik J., Molenda J., Simon D.R., Kelder E.M., Schoonman J. Conduction mechanism in operating a $LiMn_2O_4$ cathode. *Solid State Ion*. 2002. **146**(3-4): 225.
31. Bard A.J., Faulkner L.R. *Electrochemical Methods: Fundamentals and Applications*. (NY: John Wiley & Sons, 2001).
32. Sun D., Tan Z., Tian X., Ke F., Wu Y., Zhang J. Graphene: A promising candidate for charge regulation in high-performance lithium-ion batteries. *Nano Res*. 2021. **14**(12): 4370.

33. Thackeray M.M., De Kock A., Rossouw M.H., Liles D., Bittihn R., Hoge D. Spinel electrodes from the Li□Mn□O system for rechargeable lithium battery applications. J. Electrochem. Soc. 1992. **139**: 363.
34. Potapenko A.V., Kirillov S.A. Enhancing high-rate electrochemical properties of $LiMn_2O_4$ in a $LiMn_2O_4/LiNi_{0.5}Mn_{1.5}O_4$ core/shell composite. *Electrochim. Acta*. 2017. **258**: 9.
35. Yang S., Song H., Chen X. Electrochemical performance of expanded mesocarbon microbeads as anode material for lithium-ion batteries. *Electrochem. Commun*. 2006. **8**(1): 137.
36. Chen Y., Tian Y., Qiu Y., Liu Z., He H., Li B., Cao H. Synthesis and superior cathode performance of sandwiched $LiMn_2O_4$@rGO nanocomposites for lithium-ion batteries. *Mater. Today Adv*. 2019. **1**: 100001.
37. Li A., Shao Z., Yang S., Li X., Zhang A. Precipitation synthesis and enhanced electrochemical performance of graphene-modified $LiMn_2O_4$ for lithium-ion batteries. *Ionics*. 2020. **26**: 3231.

КОМПОЗИТИ $LiMn_2O_4$/ГРАФЕН ДЛЯ ЛІТІЙ-ІОННИХ АКУМУЛЯТОРІВ З ВИСОКИМИ ЕЛЕКТРОХІМІЧНИМИ ВЛАСТИВОСТЯМИ

Ю.В. Шматок, Н.І. Глоба, В.А. Сірош, С.О. Кириллов

Міжвідомче відділення електрохімічної енергетики НАН України,
бульвар Вернадського, 38А, 03680, м. Київ, Україна, e-mail: yu.shmatok@gmail.com

Покращення електрохімічних характеристик літій-манганової шпінелі $LiMn_2O_4$ є одним із найважливіших завдань для дослідників у галузі літій-іонних акумуляторів. Графенові матеріали можуть позитивно впливати на функціональні характеристики композитних електродів на основі $LiMn_2O_4$ завдяки своїм унікальним властивостям. Тому нами були досліджені композитні електроди на основі шпінелі $LiMn_2O_4$ з комерційними зразками графенів. Методами рентгенофазового аналізу, скануючої електронної мікроскопії та адсорбції–десорбції азоту досліджено структурні, морфологічні та поверхневі характеристики зразків $LiMn_2O_4$ та графену. Електрохімічні випробування композитних електродів проводили в дискових елементах CR2016 з металевим літієвим анодом. Показано, що природа $LiMn_2O_4$ є основним фактором, який визначає електрохімічну поведінку композитних електродів з точки зору їх стабільності при циклуванні та швидкісних характеристик. При цьому вплив типу графену в межах однієї шпінелі відносно невеликий, але його наявність важлива для забезпечення необхідного рівня провідності електродної структури. Незважаючи на нижчу початкову питому ємність, композити зі шпінеллю $LiMn_2O_4$, синтезованою за допомогою цитратного методу синтезу, демонструють кращу циклічну стабільність і більш високі струми розряду до 40 С порівняно з композитами на основі $LiMn_2O_4$, синтезованої твердофазним методом. Отримані електрохімічні характеристики добре узгоджуються з результатами електрохімічної імпедансної спектроскопії.

Ключові слова: *літій-манганова шпінель, графен, композитний електрод, перенесення заряду, циклувальна здатність, швидкісні характеристики, струм обміну.*